Edinburgh Research Explorer

Quantitative Proteomics Using SILAC Coupled to LC-MS/MS Reveals Changes in the Nucleolar Proteome in Influenza A Virus-Infected Cells

Link:
Link to publication record in Edinburgh Research Explorer

Document Version:
Early version, also known as pre-print

Published In:
Journal Of Proteome Research

OPEN ACCESS

Quantitative Proteomics Using SILAC Coupled to LC−MS/MS Reveals Changes in the Nucleolar Proteome in Influenza A Virus-Infected Cells

Edward Emmott,[†,‡,§] Helen Wise,[†,‖] Eva M. Loucaides,[‖] David A. Matthews,[⊥] Paul Digard,*[,‖] and Julian A. Hiscox*[,‡,§]

Institute of Molecular and Cellular Biology, Faculty of Biological Sciences, University of Leeds, LS2 9JT, United Kingdom, Astbury Centre for Structural Molecular Biology, University of Leeds, LS2 9JT, United Kingdom, Division of Virology, Department of Pathology, University of Cambridge, CB2 1QP, United Kingdom, and Department of Cellular and Molecular Medicine, School of Medical Sciences, University of Bristol, BS8 1TD, United Kingdom

Influenza A virus (IAV) is a major human pathogen whose genotypic diversity results in unpredictable pandemics and epidemics. Interaction with the cell nucleus is essential to IAV infection, allowing recruitment of cellular components to facilitate virus replication. Viral proteins are also targeted to the nucleolus, a subnuclear structure involved in ribosomal biogenesis, RNA maturation, stress response, and control of cell growth, but the functional consequences of this are unclear. We took an unbiased approach to studying IAV−nucleolar interactions by using stable isotope labeling with amino acids in cell culture (SILAC) in conjunction with LC−MS/MS to quantify changes in the nucleolar proteome following infection with A/PR/8/34 (H1N1) and A/Udorn/72 (H3N2) strains of the virus. Only a minority of nucleolar proteins showed significant changes in abundance after infection; these alterations were mostly different between the two strains but could be validated by confocal microscopy of infected cells. Many of the affected proteins comprised functional groupings, including components of ribonuclease P, RNA polymerase I, the MLL1 histone methyltransferase complex, as well as nuclear paraspeckles and the RNA editing apparatus. This, as well as comparison with other viruses that cause changes in the nucleolar proteome, suggests that IAV targets specific nucleolar pathways.

Keywords: influenza virus • nucleolus • quantitative proteomics • SILAC • LC−MS/MS • Rnase P • ADAR1 • elongation factor gamma • WDR18 • H1N1

Introduction

Influenza A virus (IAV) is one of the world's major uncontrolled pathogens, causing seasonal epidemics as well as global pandemics.[1] The negative-sense RNA of the IAV genome is divided into eight segments, and this segmentation defines many of the characteristics of the virus. Notably, reassortment of segments from different viruses coinfecting a single host has been responsible for the emergence of at least three pandemic strains within the last century.[2,3] The eight IAV segments encode 12 identified polypeptides, only two of which are nonessential outside of the laboratory setting.[4,5] Essential structural proteins include the three subunits of an RNA-dependent RNA polymerase (PB1, PB2 and PA) and a nucleoprotein (NP) that encapsidate the genomic segments into ribonucleoprotein (RNP) complexes,[6] three trans-membrane proteins (HA, NA and M2), as well as matrix (M1) and NS2/NEP.[7] Non structural proteins include NS1, the major viral antagonist of innate immune responses[8] and the two non essential proteins identified to date (both encoded by segment 2); PB1-N40, a truncated form of PB1, and PB1-F2, a pro-apoptotic virulence factor.[4,5]

Viral RNA synthesis occurs in nuclei of infected cells. Genome transcription produces capped and polyadenylated mRNAs while the vRNAs are replicated via an alternative plus sense "cRNA" intermediate.[9] Although RNPs contain the minimum essential viral components for these processes, multiple cellular factors are likely to be co-opted *in vivo.*[10,11] Viral RNA synthesis occurs in the nucleoplasm, probably partly in association with cellular RNA polymerase II.[12] However, similarly to many other RNA viruses,[13] several influenza virus proteins, including components of the polymerase, NP, NS1 and NEP have been shown to localize to the nucleolus.[14−18] The nucleolus is a dynamic subnuclear compartment involved in riboso-

mal subunit biogenesis, RNA processing and trafficking, regulation of cell growth, and response to cell stress and is composed of a complex network of protein−protein and protein−nucleic acid interactions.[19] There is evidence that virus infection can cause changes in the nuclear proteome and architecture, which may regulate its function.[20−22] Intriguingly, the nucleolus in *Caenorhabditis elegans* has recently been implicated in regulating innate immune responses against bacterial pathogens,[23] but it is not yet certain whether the mammalian nucleolus plays a defensive role against viruses.

IAV infection results in perturbations to nucleolar structure,[11,15,24] but the functional consequences of this, for virus or cell, are unknown. On one hand, the nucleolus might be functionally irrelevant to the virus, with viral RNA-binding proteins coincidentally localizing to a RNA-rich compartment. Additionally, perturbations seen to nucleolar structure may result from indirect effects of infection, such as cellular stress. However, a more interesting and evolutionary plausible hypothesis holds that even given an originally fortuitous localization of a viral protein to the nucleolus, variants where this resulted in beneficial disruption of nucleolar function and/or recruitment of nucleolar components to viral processes would be selected.[13,22] Consistent with this, a recent study showing the displacement of nucleophosmin (NPM, B23.1) from the nucleolus on IAV infection proposed a consequent stimulatory effect on viral RNA synthesis.[25] Further complicating the picture of the interaction of IAV with the nucleolus is that the nucleolar localization of viral proteins, specifically NS1 protein, may be dependent not only on the subtype of the virus[26,27] but also on the host cell.[28] For example, the NS1 protein of the A/Udorn/72 (Udorn) strain localized to the nucleolus in A549 cells, whereas A/Puerto Rico/8/34 (PR8) NS1 strain did not.[28] In contrast, NS1 from both viruses was present in the nucleolus of infected duck embryonic fibroblasts. However, study of the localization of proteins to the nucleolus using indirect immunofluorescence is complicated by poor antibody penetration and antigen abundance in the nucleolus,[29] while the addition of fluorescent tags may affect protein localization and function.

Thus, there are many unresolved questions regarding the interaction of IAV and the nucleolus. To further investigate this area of virus-cell biology, we took an unbiased approach using stable isotope labeling with amino acids in cell culture (SILAC) in conjunction with LC−MS/MS to identify and quantify cellular and viral proteins from purified nucleoli, following infection with Udorn or PR8 strains of virus, compared to mock infection. Although the virus strain exerted a large influence on the outcome, only a minority of cellular proteins showed substantial changes in abundance after infection. Furthermore, clear functional groupings of many of the affected proteins were evident, including components of ribonuclease P, RNA polymerase I, the MLL1 complex, as well as nuclear paraspeckles and the RNA editing apparatus. Overall, our data support the hypothesis of specific functional interactions between IAV and the nucleolus, rather than a global change in nucleolar integrity.

Experimental Procedures

Virus Growth. Human embryonic kidney 293-T cells[30] were cultured as previously described.[31] For viruses, a variant of the National Institute for Biological Standards and Control (UK) strain of PR8 virus that had been further adapted for growth in MDCK cells before cloning[32] and a filamentous lineage of Udorn virus (A/Udorn/301/72)[33,34] were used. Both viruses replicate productively in 293-T cells.[35] Virus stocks were grown

in embryonated eggs and titerd as previously described.[36] Virus infections were carried out at an MOI of 5 and uninfected allantoic fluid was used for mock infections. All work with infectious virus was carried out at Biosafety Level 2 (BSL-2).

Plasmids and Transfection. Adherent subconfluent 293-T cells were transfected on glass coverslips with 800 ng of phPOP1 (which expresses a vesicular stomatitis virus-tagged protein, a kind gift from G. Prujin[37]) using 1 μL of Lipofectamine 2000 (Invitrogen) in Optimem (Invitrogen). The next day, the cells were infected or mock infected before fixation and processing for immunofluorescence.

Antisera and Western Blotting. Rabbit anti-PB1 (V19), anti-PB2 (2N580), anti-PA (V35), anti-NP (A2915), anti-M1, and anti-NS1 sera have been described previously.[38−40] Anti-NS2 and anti-PB1-F2 sera were the kind gifts of Drs Agustin Portela and Jonathan Yewdell respectively. Anti-RPA43 was a rhodamine conjugated antibody raised in sheep. Mouse monoclonal anti-hnRNP M (RPM), adenosine deaminase acting on RNA 1 (ADAR1), nucleolin, fibrillarin, hnRNP A1, alpha-tubulin, beta-tubulin, GAPDH and nucleophosmin (NPM) were purchased from Abcam. Secondary antibodies were purchased from Molecular Probes, LiCor Biosciences, Sigma or DAKO. Cell lysates were analyzed by SDS-PAGE and Western blotting according to standard procedures. Blots were imaged by fluorescence using IRDye 700/800 conjugated secondary antibodies on a Licor Biosciences Odyssey near-infrared imaging platform.

Confocal Microscopy. For confocal microscopy, cells were fixed in 4% formaldehyde, permeabilised with 0.2% Triton X100 in phosphate buffered saline and probed with the desired combinations of primary and secondary antibodies as previously described.[34] Images (single optical sections) were captured sequentially on a Leica TCS-NT or DMI 4000 confocal microscope and processed for daylight display using Adobe Photoshop.

Growth of Cells for SILAC and Subcellular Fractionation. 293-T cells were maintained in stable isotope-labeled Dulbecco's modified Eagle's medium (Dundee Cell products) supplemented with 10% dialyzed fetal bovine serum (Dundee Cell Products), penicillin/streptomycin and incubated at 37 °C in the presence of 5% CO_2. Cells were grown in stable isotope-labeled growth media containing "light" (R0K0), "medium" (R6K4) or "heavy" (R10K8) arginine and lysine for a period of 2 weeks prior to infection. Twenty-five million cells were seeded into 500 cm^2 dishes and grown for 24 h at which point cells were infected with virus or mock-infected with allantoic fluid. At 10 h postinfection, cells were harvested. (Note that both viruses productively infect 293-T cells, under these conditions of single cycle growth. PR8 strain replicates to around 1×10^7 PFU/mL while, as expected for a filamentous strain, Udorn replicates slightly less to around 1×10^6 PFU/mL.) Subcellular fractionation was carried out as described[42] with the following modifications: Incubation time in buffer A prior to dounce homogenization was increased to 10 min, the number of dounce homogenization strokes was decreased to 8, and the number of sonication repeats increased to 8.

Gel Electrophoresis and In-Gel Digestion. Each sample was reduced in SDS-PAGE loading buffer containing 10 mM DTT and alkylated in 50 mM iodoacetamide prior to being boiled and then separated by one-dimensional SDS-PAGE (4−12% Bis-Tris Novex mini-gel, Invitrogen) and visualized by colloidal Coomassie staining (Novex, Invitrogen). The entire protein gel lane was excised and cut into 10 gel slices each. Gel slices were

subjected to in-gel digestion with trypsin.[41] The resulting tryptic peptides were extracted by 1% formic acid, acetonitrile, lyophilized in a Speedvac (Helena Biosciences) and resuspended in 1% formic acid.

LC−MS/MS. LC−MS/MS was performed by Dundee Cell Products Ltd. Trypsin digested peptides were separated using an Ultimate U3000 (Dionex Corporation) nanoflow LC−system consisting of a solvent degasser, micro and nanoflow pumps, flow control module, UV detector and a thermostatted autosampler. Ten microliters of sample (a total of 2 μg) was loaded with a constant flow of 20 μL/min onto a PepMap C18 trap column (0.3 mm id × 5 mm, Dionex Corporation). After trap enrichment peptides were eluted off onto a PepMap C18 nano column (75 mm × 15 cm, Dionex Corporation) with a linear gradient of 5−35% solvent B (90% acetonitrile with 0.1% formic acid) over 65 min with a constant flow of 300 nL/min. The HPLC system was coupled to a LTQ Orbitrap XL (Thermo Fisher Scientific Inc.) via a nano ES ion source (Proxeon Biosystems). The spray voltage was set to 1.2 kV and the temperature of the heated capillary was set to 200 °C. Full scan MS survey spectra (m/z 335−1800) in profile mode were acquired in the Orbitrap with a resolution of 60 000 after accumulation of 500 000 ions. The five most intense peptide ions from the preview scan in the Orbitrap were fragmented by collision-induced dissociation (normalized collision energy 35%, activation Q 0.250 and activation time 30 ms) in the LTQ after the accumulation of 10 000 ions. Maximal filling times were 1000 ms for the full scans and 150 ms for the MS/MS scans. Precursor ion charge state screening was enabled and all unassigned charge states as well as singly charged species were rejected. The dynamic exclusion list was restricted to a maximum of 500 entries with a maximum retention period of 90 s and a relative mass window of 10 ppm. The lock mass option was enabled for survey scans to improve mass accuracy.[42] The data were acquired using Xcalibur software.

Quantification and Bioinformatics Analysis. Quantification was performed with MaxQuant version 1.0.7.4[43] and was based on two-dimensional centroid of the isotope clusters within each SILAC pair. To minimize the effect of outliers, protein ratios were calculated as the median of all SILAC pair ratios that belonged to peptides contained in the protein. The percentage variability of the quantitation was defined as the standard deviation of the natural logarithm of all ratios used for obtaining the protein ratio multiplied by a constant factor 100.

The generation of peak list, SILAC- and extracted ion current-based quantitation, calculated posterior error probability, and false discovery rate based on search engine results, peptide to protein group assembly, and data filtration and presentation was carried out using MaxQuant. The derived peak list was searched with the Mascot search engine (version 2.1.04; Matrix Science, London, U.K.) against a concatenated database combining 80 412 proteins from International Protein Index (IPI) human protein database version 3.6 (forward database), and the reversed sequences of all proteins (reverse database). Alternatively, database searches were done using Mascot (Matrix Science) as the database search engine and the results saved as a peptide summary before quantification using MSQuant (http://msquant.sourceforge.net/). Parameters allowed included up to three missed cleavages and two labeled amino acids (arginine and lysine). Initial mass deviation of precursor ion and fragment ions were up to 7 ppm and 0.5 Da, respectively. The minimum required peptide length was set to 6 amino acids. To pass statistical evaluation, posterior error probability (PEP) for peptide identification (MS/MS spectra) should be below or equal to 0.1. The required false positive rate (FPR) was set to 5% at the peptide level. False positive rates or PEP for peptides were calculated by recording the Mascot score and peptide sequence length-dependent histograms of forward and reverse hits separately and then using Bayes' theorem in deriving the probability of a false identification for a given top scoring peptide. At the protein level, the false discovery rate (FDR) was calculated as the product of the PEP of a protein's peptides where only peptides with distinct sequences were taken into account. Proteins were quantified if at least one MaxQuant-quantifiable SILAC pair was present. Identification was set to a false discovery rate of 1% with a minimum of two quantifiable peptides. The set value for FPR/PEP at the peptide level ensures that the worst identified peptide has a probability of 0.05 of being false; and proteins are sorted by the product of the false positive rates of their peptides where only peptides with distinct sequences are recognized. During the search, proteins are successively included starting with the best-identified ones until a false discovery rate of 1% is reached; an estimation based on the fraction of reverse protein hits. Enzyme specificity was set to trypsin allowing for cleavage of N-terminal to proline and between aspartic acid and proline. Carbamidomethylation of cysteine was searched as a fixed modification, whereas N-acetyl protein and oxidation of methionine were searched as variable modifications.

Data were analyzed through the use of Ingenuity Pathways Analysis (Ingenuity Systems, www.ingenuity.com). Networks and functional groupings were generated using data sets containing gene identifiers and corresponding expression values and uploaded into the application.

Results and Discussion

Proteomic Overview of the Effects of IAV Infection on the Nucleolus. To provide a global view of the interaction of IAV with the nucleolus quantitative proteomics using SILAC-coupled to LC−MS/MS was employed. This analysis was conducted once and a target list of cellular proteins whose abundance changed in IAV-infected cells derived obtained. The differential abundance of these proteins was then confirmed using independent techniques including Western blot analysis and confocal microscopy. In order to conduct the SILAC analysis, 293-T cells were grown for six doubling times in either light (R0K0), medium (R6K4) or heavy (R10K8) labeled media before being infected with PR8, mock infected or infected with Udorn virus respectively. PR8 is a human H1N1 isolate whose passage history is now uncertain but is generally regarded as heavily laboratory adapted, with the properties of high growth yields in many culture systems as well as high pathogenicity in mice.[32,44] Udorn virus is a human H3N2 isolate that retains the filamentous morphology associated with low passage clinical isolates.[31,34] Ten hours postinfection cells were enriched into cytoplasmic, nucleoplasmic or nucleolar fractions as described.[45] To validate the fractionation process, the distribution of marker proteins for each cellular compartment was examined by Western blotting, revealing acceptable levels of purity (Figure 1). The subcellular localization of each of the nontransmembrane IAV proteins was also examined (Figure 2A). Overall, similar levels of the viral proteins were seen in samples from Udorn and PR8 infected cells, confirming successful infection with both viruses. Most viral proteins were detected to some extent in each of the three subcellular
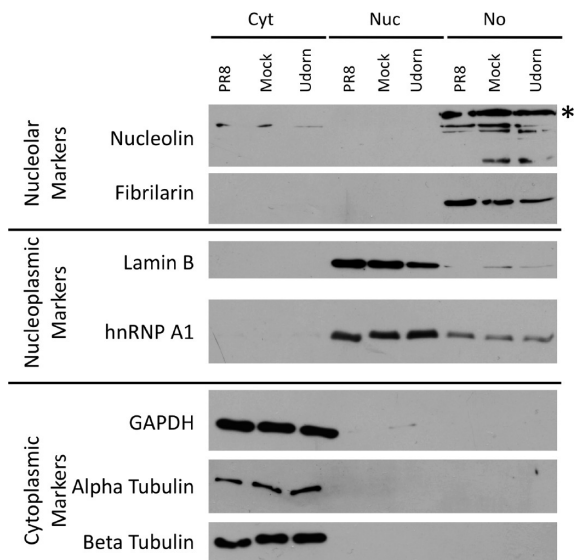
Figure 1. Western blot analysis of the distribution of marker proteins for cytoplasmic (Cyt) (GAPDH, alpha-tubulin and beta-tubulin), nuclear (Nuc) (Lamin B and hnRNP A1) and nucleolar extracts (No) (nucleolin and fibrillarin) from mock or virus infected cells. *Indicates the expected position of full-length nucleolin, the faster migrating species are likely to be autocatalytic breakdown products.[69]

Figure 2. Western blot analysis of the distribution of (A) non-transmembrane IAV PR8 (PR8) and Udorn (Ud) proteins and (B) selected cellular nucleolar proteins identified in the LC−MS/MS analysis between cytoplasmic (Cyt), nuclear (Nu) and nucleolar (No) fractions. The PB1-F2 and NEP polypeptides are highlighted with asterisks to distinguish them from cross-reactive cellular polypeptides with similar electrophoretic mobilities. Note also that the NS1 and NEP proteins of PR8 and Udorn viruses display slightly different electrophoretic mobility. The apparent discrepancy in migration between the PR8 and Udorn PB1 polypeptides in the nucleolar fraction was not seen in replicate gels and is most likely an artifact.

fractions, with the possible exceptions of NEP, PB1-F2 and PB1-N40. In the case of NEP and PB1-F2, cross-reactivity of the antibodies with cellular components with similar electrophoretic mobilities found in nuclear and/or nucleolar fractions as well as failure of the Udorn PB1-F2 to react with the antiserum, prevented their unambiguous detection. The low abundance PB1-N40 was mostly resident in the cytoplasm, consistent with previous observations.[5]

However, the relative proportions of the viral proteins present in each fraction varied, with the NP and NS1 polypeptides showing higher levels of nucleolar accumulation than the M1 or polymerase subunits, again, consistent with previous observations.[14−17,26,28,46] Some differences were also observed between the distributions of the PR8 and Udorn polypeptides: the PR8 NS1 was notably more cytoplasmic than in Udorn infection, consistent with the strain-dependent differences noted previously for Udorn NS1 and the A/WSN/33 virus,[26] which like PR8 NS1, lacks a second nuclear localization signal. Smaller fluctuations in the degree of nucleolar association were also seen for two NS1 polypeptides, as well as for M1, PB2 and NEP. Next, the nucleolar fractions were analyzed by mass spectrometry. Four viral proteins (HA, NP, M1 and NS1) were identified by LC−MS/MS for the PR8 strain and six (PB2, HA, NP, M1, NS1 and NS2) for the Udorn strain (Table 1).

This was broadly consistent with the outcome of the Western blotting experiments, though the identification of the glycoprotein HA as a nucleolar resident protein was unexpected and may reflect contamination. Four-hundred thirty-eight cellular proteins were identified and quantified in all three experimental conditions. These proteins were then compared to the nucleolar proteome database and Uniprot annotation in order to confirm classification as nucleolar and eliminate known contaminants such as voltage dependent anion-selective (VDAC) proteins. This reduced the data set to 348 proteins identified and quantified (Supplementary Table 1, Supporting Information). The nucleolar proteome of 293-T cells contained proteins
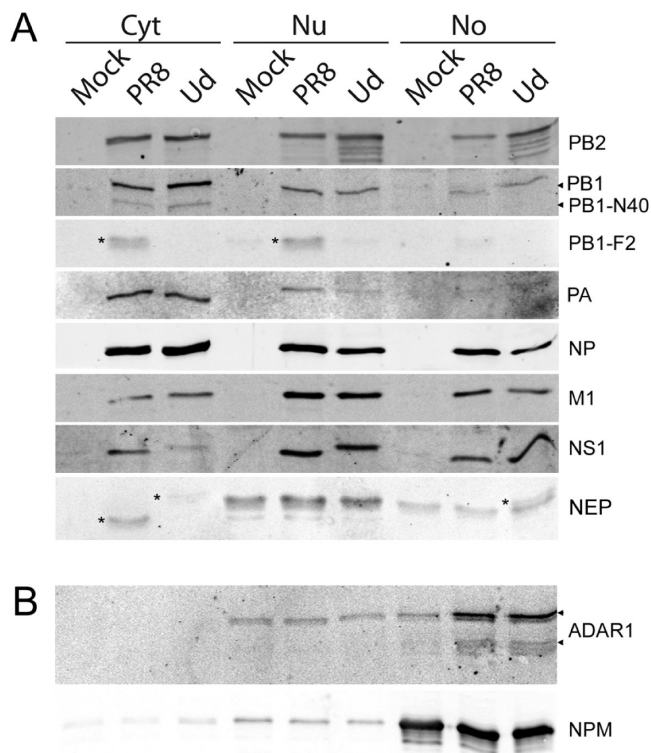
associated with RNA post-transcriptional modification, gene expression, DNA recombination and repair, cellular growth and proliferation and protein synthesis and is similar to other nucleolar proteomes that have been published for other cell types[45,47,48] (Figure 3).

For quantitative analysis of differences between paired experimental samples, previous investigations using SILAC and LC−MS/MS have applied ratio cutoffs ranging from near 1.3 to 2.0 fold.[49] We chose a 2.0-fold cut off as a basis for investigating potential significant changes between data sets through Ingenuity Pathway Analysis and to provide a basis for comparing the current data set to previous studies.[21,45,50] Even by this relatively strict criterion, the nucleolar abundance of several cellular proteins were significantly altered in cells infected with both strains of IAV (Udorn strain, Table 2; PR8 strain, Table 3).

However, clear differences were seen in the changes to the nucleolar proteome induced by the two viruses. The majority of the greater than 2-fold changes in abundance resulting from Udorn infection involved loss of proteins from the nucleolus (21 polypeptides, versus one showing increased nucleolar residence). Inspection of the proteins depleted from the nucleolus revealed some notable groupings. The largest set (5 members; Table 2) were all components of RNase P. The three

Table 1. Influenza A Virus Proteins Identified from Nucleolar Fractions[a]

name	gene identifier (GI) number	peptides	% sequence coverage	PEP	protein function
			A/Puerto Rico/8/1934 Strain		
HA	gi126599270	3	5.3	5.2×10^{-11}	Surface glycoprotein, interacts with receptor.
NP	gi126599284	26	58.6	2.4×10^{-205}	Encapsidate the virus genome.
M1	gi126599292	14	75.4	1.7×10^{-101}	Role in virus entry and assembly.
NS1	gi126599211	13	64.3	6.5×10^{-156}	Inhibits post-transcriptional processing of cellular pre-mRNA.
			A/Udorn/307/1972		
PB2	gi18615852	6	10.8	8.4×10^{-38}	Viral transcription initiation and cap-snatching.
HA	gi18615858	6	11.5	6.5×10^{-42}	Surface glycoprotein, interacts with receptor.
NP	gi18615860	24	49	2.2×10^{-141}	Encapsidate the virus genome.
M1	gi18615864	13	67.1	4.3×10^{-83}	Role in virus entry and assembly.
NS1	gi18615868	21	84.8	6.8×10^{-296}	Inhibits post-transcriptional processing of cellular pre-mRNA.
NS2	gi18615870	13	28.1	4.5×10^{-10}	Nuclear export of encapsidated genomic RNAs.

[a] Detailed are the viral protein name, gene identifier number, number of peptides for identification, the sequence coverage on the viral protein this represents and the posterior error probability (PEP) score, which is a probability that an individual match is a chance event.
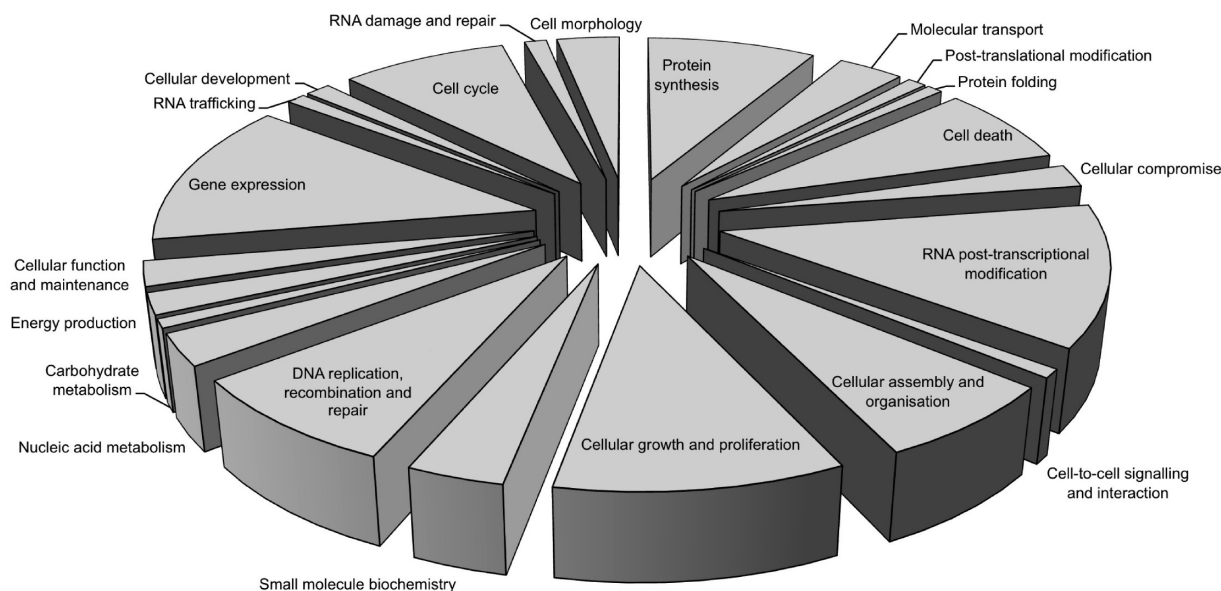

Figure 3. Ingenuity Pathway Analysis of the nucleolar proteome in 293-T cells showing the relative proportion of each functional category of proteins.

major components of nuclear paraspeckles (Table 2) also showed significant reductions in nucleolar residence, as did three subunits of the MLL1 histone H3 methyltransferase complex and two subunits of RNA polymerase I. Interestingly, the para-speckle protein SFPQ has been previously shown to interact with the IAV polymerase,[51] while the heat shock proteins HSPA8 and the WD repeat protein, WDR18, were identified as important for IAV replication in RNAi screens for essential host factors.[52−54] In contrast, PR8 infection did not result in major loss of any detected protein (using the 2-fold criterion), but instead caused the increased nucleolar association of 3 cellular proteins (Table 3). Two of these proteins were in common with the Udorn data set: nucleolar resident ADAR1 increased nearly 3-fold after infection with both viruses, but while the Lupus La autoantigen was depleted from the nucleolus after Udorn infection, it increased in PR8-infected cells. The third protein showing a 2-fold increased nucleolar abundance in PR8 infected cells was a polypeptide similar to Elongation factor gamma (Table 3). This protein also increased in the nucleolus after Udorn infection, but although it showed the second highest enrichment after ADAR1, this was only 1.6-fold

(Supplementary Table 1, Supporting Information). Other similarities between the effects of Udorn and PR8 infection were evident if lower stringency criteria were used to draw a cutoff: WDR18 was the fifth most depleted protein identified from PR8 nucleoli (ratio of −1.4), while the POP5 subunit of RNaseP showed a ratio of −1.3 (Supplementary Table 1, Supporting Information). However, the most reduced proteins (ratios of 1.4 to −1.6) were hnRNP proteins and splicing factors (Supplementary Table 1, Supporting Information). This included a subunit of splicing factor 3B (SF3B; ratio of −1.5) previously identified as important for IAV replication.[54,55]

Validation of the SILAC and LC−MS/MS Data. Next, we validated the outcome of the SILAC and LC−MS/MS data by examining the response of selected cellular proteins to viral infection by Western blotting and/or confocal microscopy, testing proteins that showed an increased, no change or decreased abundance in the nucleolus in response to IAV infection. One protein whose nucleolar abundance was increased after infection with both viruses was ADAR1 protein (Tables 2 and 3). ADAR1 is an interferon-inducible RNA-editing protein with a potential role in innate antiviral immunity,

Table 2. Cellular Proteins Showing ≥ 2-Fold Changes in Abundance Following Infection with IAV (Strain Udorn)[a]

name	IPI no.	complex	ratio	pept	%SC	PEP	protein function(s)
				Proteins showing increased abundance			
ADAR1	IPI00394668	PSE	2.8	19	18.4	3.7×10^{-147}	RNA editing, converts adenosines to inosines. May be responsible for hypermutation of RNA viruses.
				Proteins showing decreased abundance			
PSPC1	IPI00103525	PSE	−2.1	9	14.5	9.1×10^{-10}	Regulates gene transcription with NONO and SFPQ. Binds to poly(A), poly(G) and poly(U) in RNA.
SFPQ	IPI00010740	PSE	−2.5	23	34.8	5.4×10^{-202}	DNA and RNA binding protein required in early spliceosome formation.
NONO	IPI00304596	PSE	−2.5	34	55.8	3.3×10^{-198}	DNA and RNA binding protein involved in pre-mRNA splicing. Together with NONO may be involved in retention of defective RNAs.
PELP1	IPI00006702	MLL1	−2.0	7	8.6	9.0×10^{-16}	Role in E2-mediated cell cycle progression by interacting with RB1.
TEX10	IPI00549664	MLL1	−2.1	3	4.8	2.1×10^{-14}	Unknown.
LAS1L	IPI00641990	MLL1	−2.2	8	14.9	1.1×10^{-83}	Unknown.
Ribonuclease P	IPI00478229	RNaseP	−2.0	4	18	1.5×10^{-47}	Generates mature tRNAs.
POP1	IPI00293331	RNaseP	−2.1	2	2.8	0.001	Removes 5′-extra nucleotides from tRNA precursor.
POP5	IPI00107563	RNaseP	−2.0	3	19	0.0001	Removes 5′-extra nucleotides from tRNA precursor.
POP7	IPI00027142	RNaseP	−2.1	2	24.3	1.8×10^{-24}	Removes 5′-extra nucleotides from tRNA precursor.
RPP14	IPI00215966	RNaseP	−2.1	2	27.4	7.1×10^{-19}	Removes 5′-extra nucleotides from tRNA precursor.
POLR1B	IPI00418797	RNAPI	−2.0	4	4.9	5.1×10^{-24}	Core component and contributes to catalytic activity.
RPA43	IPI00005477	RNAPI	−2.1	2	8.3	2.6×10^{-07}	Recruitment of Pol I to rDNA promoters.
HSPA8	IPI00003865		−2.0	5	9.8	1.6×10^{-16}	ATP binding belongs to HSP70 family.
RPL24	IPI00873403		−2.0	2	12.7	8.9×10^{-10}	Ribosomal protein.
C16orf88	IPI00554560		−2.0	3	8.5	2.3×10^{-08}	Unknown.
WDR18	IPI00032533		−2.1	7	17.4	2.2×10^{-35}	Unknown.
C6orf153	IPI00106638		−2.2	4	18.5	1.9×10^{-24}	Ribosome biogenesis and rRNA processing.
Lupus La	IPI00009032		−2.3	2	7.1	9.8×10^{-11}	Transcription of RNA pol III.
NOL9	IPI00002902		−2.5	7	14.1	1.2×10^{-28}	Unknown.
UTP23	IPI00031612		−2.8	2	9.2	0.002	Ribosome biogenesis and rRNA processing.

[a] Shown is the protein name, International Protein Index number, (for selected cases) the functional complex/group it falls in, protein ratio in infected versus mock infected nucleoli, number of peptides used to identify the protein (Pept), the sequence coverage on the protein this represents (%SC) and the PEP score. Abreviations for functional complexes are: PS/E, paraspeckles/A-I RNA editing; MLL1, Components of the MLL1 histone H3 methyltransferase complex; RNAseP, RNAse P components; RNAPI, RNA polymerase I.

Table 3. Cellular Proteins Showing ≥ 2-Fold Changes in Abundance Following Infection with Influenza Virus (Strain PR8)[a]

name	IPI no.	complex	ratio	pept	%SC	PEP	protein function(s)
ADAR1	IPI00394668	PS/E	2.9	19	18.4	3.7×10^{-147}	RNA editing, converts adenosines to inosines. May be responsible for hypermutation of RNA viruses.
Lupus La	IPI00009032		3.3	2	7.1	9.8×10^{-11}	Transcription of RNA pol III.
Similar to EF1 gamma	IPI00000875		2.0	5	12.1	1.8×10^{-37}	Translation elongation.

[a] Shown is the protein name, International Protein Index number, (for selected cases) the functional complex/group it falls in, protein ratio in infected versus mock infected nucleoli, number of peptides used to identify the protein, the sequence coverage on the protein this represents and the PEP score. Abbreviations for functional complexes are: PS/E, paraspeckles/A-I RNA editing.
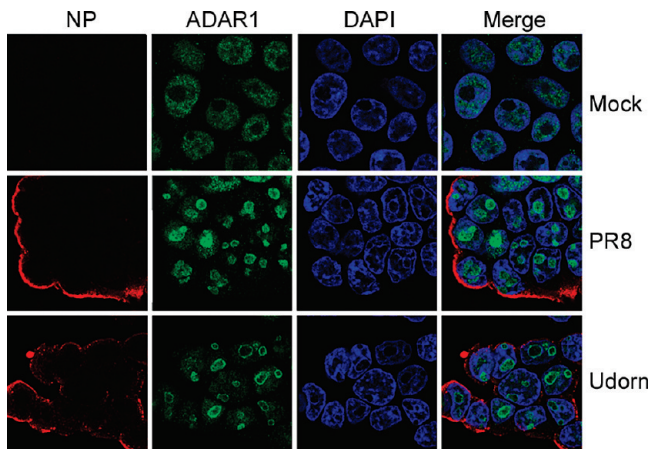
Figure 4. Indirect immunofluorescence confocal microscopy analysis of the subcellular localization of ADAR1 in mock-infected and infected (PR8 and Udorn) cells at 12 h p.i. IAV NP is shown in red, ADAR1 in green, the nucleus is stained with DAPI (blue) and a merge image is presented. Note that NP localizes to the apical plasma membrane late in infection and is therefore only seen at the periphery of cell clumps in the optical sections shown.
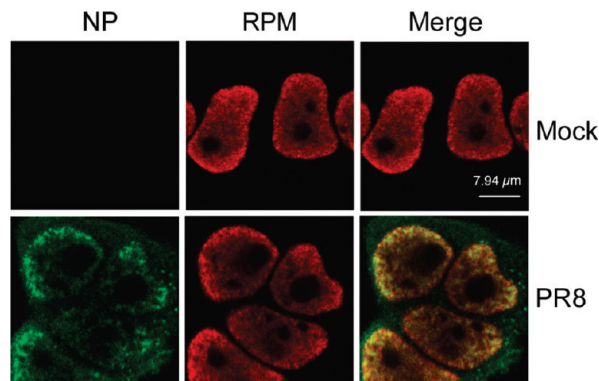

Figure 5. Indirect immunofluorescence confocal microscopy analysis of the subcellular localization of RPM in mock-infected and PR8 infected cells at 8 h p.i. IAV NP is shown in green, RPM in red, and a merge image is presented.
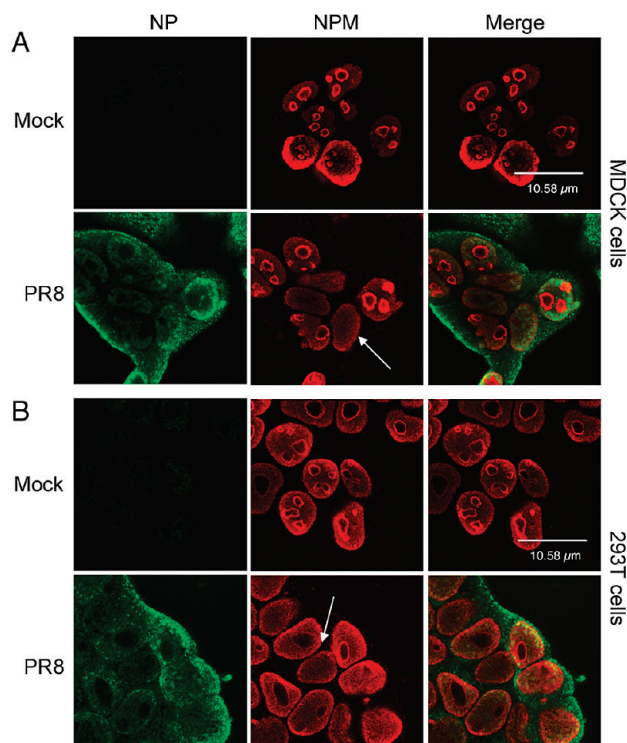

Figure 6. Indirect immunofluorescence confocal microscopy analysis of the distribution of NPM (red) in mock and PR8-infected (green) (A) MDCK and (B) 293-T cells at 11 h p.i. Arrows highlight examples of cells where nucleolar NPM staining is lost.

including against IAV, and which has also been reported to interact with NS1 protein.[56−58] Western blotting confirmed that increased amounts of both long (150 kDa) and short (110 kDa) forms of ADAR1 were seen in the nucleolar fraction from IAV infected cells (Figure 2B). When mock-infected 293-T cells were examined by confocal microscopy, ADAR1 was predominately nucleoplasmic, whereas in the majority of IAV infected cells (as delineated by positive staining for viral NP) there was a marked increase in fluorescence in the nucleolus (Figure 4), verifying the proteomic analysis.

Genetic studies in mice infected with IAV indicated that ADAR1 can edit at least one of the viral mRNAs and may be part of an antiviral response.[57] It is therefore tempting to speculate that sequestration of ADAR1 to the nucleolus in influenza virus infected cells is a mechanism to mitigate its antiviral activity.

As examples of proteins whose abundance did not change dramatically in the LC−MS/MS analysis we analyzed the subcellular localization of heterogeneous nuclear ribonucleoprotein M (RPM or hnRNP M) and NPM, both of which have been defined as interaction partners of the viral polymerase and/or RNP.[25,51] The fold changes in nucleolar abundance for RPM were −1.5 for both viruses and for NPM, 1.09 (PR8) and −1.5 (Udorn). Confocal microscopy of uninfected 293-T cells showed that RPM mostly localized to the nucleoplasm with a slight preference for the nuclear periphery (Figure 5). This pattern was unchanged after infection with PR8 virus, although reasonable colocalization was seen between NP and RPM (Figure 5). Here, the low intensity staining of the nucleolus in uninfected cells hindered identification of whether infection caused a further reduction.

Next, focusing on NPM, we investigated a potential discrepancy between our results and a previous study examining the interaction of IAV with this protein. Mayer and colleagues showed that IAV infection induced the redistribution of recombinant Flag-tagged NPM out of the nucleolus of MDCK cells at late times postinfection (6−8 h p.i.), where it partially colocalized with nuclear NP.[25] In contrast, our SILAC LC−MS/MS analysis showed little effect on the bulk localization of NPM

in the nucleolus of infected 293-T cells. First, we examined NPM distribution in the 293-T cell fractions by Western blot, which, consistent with the proteomics analysis, showed no change in nucleolar content after infection (Figure 2B). We therefore asked if we could reproduce NPM relocalization effects in infected cells by immunofluorescence, as well as testing if cell type influenced the outcome, by analyzing endogenous NPM localization in MDCK and 293-T cells infected or mock infected with PR8 virus. Although NPM has the ability to shuttle to the cytoplasm[59] it localized predominantly to the nucleolus in uninfected MDCK cells (Figure 6A), as was previously observed for Flag-NPM.[25] Occasionally, strong cytoplasmic NPM staining was detected in dividing cells as judged by DAPI staining (data not shown). NPM also localized to the nucleolus of uninfected 293-T cells but this was less pronounced than in MDCK cells
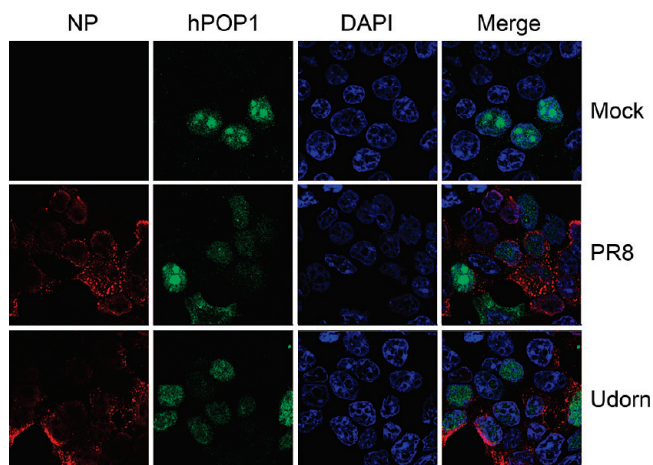
Figure 7. Indirect immunofluorescence confocal microscopy analysis of the subcellular localization of POP1 in mock-infected and infected (PR8 and Udorn) cells at 6 h p.i. IAV NP is shown in red, POP1 in green, the nucleus is stained with DAPI (blue) and a merge image is presented.

Figure 8. Indirect immunofluorescence confocal microscopy analysis of the subcellular localization of RPA43 in mock-infected and infected (PR8 and Udorn) cells at 12 h p.i. IAV NP is shown in green, RPA43 in red, the nucleus is stained with DAPI (blue) and a merge image is presented.

and higher intensity staining of the nucleoplasm was detected (Figure 6B). In both cell types no change in NPM staining was detected at early time-points of infection (data not shown). However, at 11 h p.i. nucleolar NPM localization was distinctly diminished in a subset of infected cells (indicated with white arrows, Figure 6A and B), with the effect being more pronounced in MDCK cells. A similar outcome was obtained with Udorn virus (data not shown).

Thus, we observed similar effects of infection on NPM localization to those described by Mayer et al. (2007), albeit less marked and only occurring in a fraction of infected cells. Some of these discrepancies might be accounted for by virus strain (A/WSN/33 vs PR8) or by the fact that Mayer and colleagues examined recombinant, tagged NPM and not endogenous protein.[25] However, we think the fact that we only saw relocalization of NPM in some and not all infected cells, together with the less pronounced nucleolar localization of NPM in 293-T cells accounts for the failure to detect a significant reduction in the NPM nucleolar content by SILAC analysis. We also note that a recent study also found that IAV infection only resulted in NPM relocalization in a subset of infected duck embryo fibroblasts.[28]

LC−MS/MS analysis indicated that several proteins associated with ribonuclease P (RNaseP) were decreased in abundance in the nucleolus of Udorn infected cells, including POP1 and POP5. RNaseP is a large ribonucleoprotein complex that generates mature tRNA molecules by cleaving the 5′ leader sequence of precursor tRNAs. However, there is also evidence that nuclear RNaseP is involved in the transcription of tRNA genes and other small noncoding RNAs by RNA polymerase III as well as rRNA by RNA polymerase I.[60,61] To examine the response of RNaseP polypeptides to IAV infection by microscopy, cells were transfected with a plasmid encoding a tagged form of POP1 then infected (or mock infected) with virus. In mock-infected cells, POP1 predominantly localized to the nucleolus, with some staining of the nucleoplasm, whereas in Udorn infected cells, this pattern was reversed, with often weaker signals from nucleolar regions than the nucleoplasm (Figure 7). PR8 infection also provoked some redistribution of
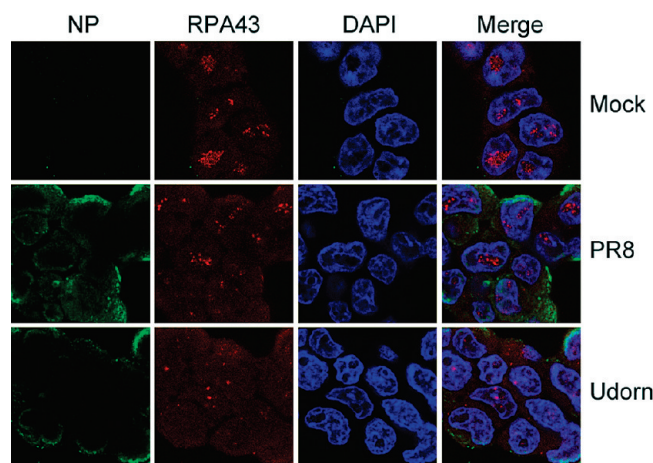
POP1, although to a less marked extent than Udorn infection. Again, these data are consistent with the mass spectrometry findings.

As a final test of the accuracy of the proteomic analysis, we examined the subcellular localization of the RPA43 subunit of RNA polymerase I after infection, as the SILAC analysis showed substantial reductions in its nucleolar residence in Udorn but not PR8 infected cells (fold changes of −2.1 versus 1.1 respectively; Table 2). Twelve h p.i. infected or mock infected cells were fixed and stained for RPA43 and NP. In uninfected cells, RPA43 displayed the expected staining pattern of prominent nucleolar foci, although it is uncertain whether the cytoplasmic staining for RPA43 is specific (Figure 8). This pattern largely persisted in PR8 infected cells although some cells showed reduced numbers and/or fainter nucleolar foci. In contrast, near complete disruption of the normal RPA43 localization was seen in Udorn infected cells, with the staining revealing very few bright foci that moreover were not universally associated with the nucleolar regions.

Overall we have tested the SILAC/mass spectrometry data by Western blotting and/or microscopy for several cellular proteins, finding good congruence between the experimental methods. This observation is in keeping with our previous analyses using SILAC coupled to LC−MS/MS and validation of data sets.[21,45,50,62] Therefore, we conclude that the SILAC database is likely to be a fair and accurate reflection of the IAV-induced changes to the nucleolar proteome. As a future analysis it would be interesting to test if the differences between the two strains correlate with the established differences between nuclear/nucleolar targeting and/or IFN-evasion activities of PR8 and H3N2 NS1 proteins.

Comparison of the Nucleolar Proteome Changes in Influenza A Virus-Infected Cells with Those of Other Viruses. The nucleolar proteome in the context of infection has been characterized for two other very different viruses; adenovirus[21] and the coronavirus infectious bronchitis virus (IBV).[45] Adenoviruses are double stranded DNA viruses that replicate in the nucleus of infected cells, whereas coronaviruses have positive stranded RNA genomes that replicate in the cytoplasm. Nevertheless, proteins from both viruses have been shown to
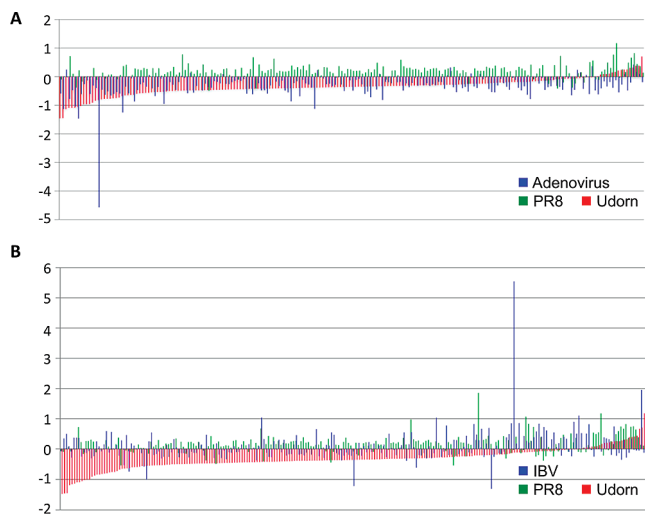
Figure 9. Fold changes (relative to uninfected cells) of (A) 199 nucleolar proteins after infection with adenovirus (blue), PR8 (green) and Udorn (red) viruses and 230 nucleolar proteins after infection with IBV (blue), PR8 (green) and Udorn (red) viruses. In this plot, a change of +1/−1 indicates a 2-fold increase or decrease in that protein's abundance in the nucleoli of an infected cell and between 0 and 1 represents no significant change in abundance between infected and uninfected cells. Thus, outwardly while opposite changes appear between the PR8 strain and adenovirus, only a few of these are greater than 2-fold.

localize to the nucleolus in infected cells.[63−68] Proteomic analysis revealed that similar to this study, global nucleolar proteome changes did not occur in adenovirus and coronavirus infected cells, and only a subset of nucleolar proteins changed in abundance.[21,45] We therefore compared the fold changes found in the set of proteins that were identified and quantified in each nucleolar proteome experiment. To this end, the proteins in common to the various experiments were sorted according to the fold change in Udorn infected cells and plotted side by side.

In general the changes seen in Udorn and adenovirus infections were somewhat more similar than between PR8 and the other two data sets (Figure 9A). However, only a very small number of proteins showed a significant change during viral infection (as defined by a 2-fold alteration in abundance) in the nucleolus of either adenovirus or IAV infected cells. That adenovirus and Udorn seem more similar may possibly reflect the observation that both cause symptomatic respiratory infections in humans, whereas PR8 does not. Further investigation will determine if this really is the case. A similar comparison of some 230 nucleolar proteins between IBV and both IAV strains revealed no major similarities (Figure 9B).

However, these data show that viral infection causes a significant change in only a small subset of nucleolar proteins. In addition, these viruses apparently disturb different aspects of the nucleolar proteome reflecting their different replication strategies and host pathogenicity. These two observations reenforce a highly significant point: viral effects on the nucleolus are targeted rather than a result of collateral damage arising from the cell eventually succumbing to infection. The data presented here suggest that at least one strain of IAV targets specific nucleolar-related pathways; further work is ongoing to test the functional significance of this.

References

(1) Webby, R. J.; Webster, R. G. Are we ready for pandemic influenza. *Science* **2003**, *302* (5650), 1519–1522.
(2) Webster, R. G.; Bean, W. J.; Gorman, O. T.; Chambers, T. M.; Kawaoka, Y. Evolution and ecology of influenza A viruses. *Microbiol. Rev.* **1992**, *56* (1), 152–179.
(3) Morens, D. M.; Taubenberger, J. K.; Fauci, A. S. The persistent legacy of the 1918 influenza virus. *N. Engl. J. Med.* **2009**, *361* (3), 225–229.
(4) Chen, W.; Calvo, P. A.; Malide, D.; Gibbs, J.; Schubert, U.; Bacik, I.; Basta, S.; O'Neill, R.; Schickli, J.; Palese, P.; Henklein, P.; Bennink, J. R.; Yewdell, J. W. A novel influenza A virus mitochondrial protein that induces cell death. *Nat. Med.* **2001**, *7* (12), 1306–1312.
(5) Wise, H. M.; Foeglein, A.; Sun, J.; Dalton, R. M.; Patel, S.; Howard, W.; Anderson, E. C.; Barclay, W. S.; Digard, P. A complicated message: Identification of a novel PB1-related protein translated from influenza A virus segment 2 mRNA. *J. Virol.* **2009**, *83* (16), 8021–8031.
(6) Portela, A.; Digard, P. The influenza virus nucleoprotein: a multifunctional RNA-binding protein pivotal to virus replication. *J. Gen. Virol.* **2002**, *83* (Pt 4), 723–734.
(7) Nayak, D. P.; Balogun, R. A.; Yamada, H.; Zhou, Z. H.; Barman, S. Influenza virus morphogenesis and budding. *Virus Res.* **2009**, *143* (2), 147–161.
(8) Hale, B. G.; Randall, R. E.; Ortin, J.; Jackson, D. The multifunctional NS1 protein of influenza A viruses. *J. Gen. Virol.* **2008**, *89* (Pt 10), 2359–2376.
(9) Neumann, G.; Brownlee, G. G.; Fodor, E.; Kawaoka, Y. Orthomyxovirus replication, transcription, and polyadenylation. *Curr. Top. Microbiol. Immunol.* **2004**, *283*, 121–143.
(10) Amorim, M. J.; Digard, P. Influenza A virus and the cell nucleus. *Vaccine* **2006**, *24* (44−46), 6651–6655.
(11) Josset, L.; Frobert, E.; Rosa-Calatrava, M. Influenza A replication and host nuclear compartments: many changes and many questions. *J. Clin. Virol.* **2008**, *43* (4), 381–390.
(12) Engelhardt, O. G.; Fodor, E. Functional association between viral and cellular transcription during influenza virus infection. *Rev. Med. Virol.* **2006**, *16* (5), 329–345.
(13) Hiscox, J. A. RNA viruses: hijacking the dynamic nucleolus. *Nat. Rev. Microbiol.* **2007**, *5*, 119–127.
(14) Dimmock, N. J. New virus-specific antigens in cells infected with influenza virus. *Virology* **1969**, *39* (2), 224–234.
(15) Ter Meulen, V.; Love, R. Virological, immunochemical, and cytochemical studies of four HeLa cell lines infected with two strains of influenza virus. *J. Virol.* **1967**, *1* (3), 626–639.
(16) Taylor, J. M.; Hampson, A. W.; Layton, J. E.; White, D. O. The polypeptides of influenza virus. IV. An analysis of nuclear accumulation. *Virology* **1970**, *42* (3), 744–752.
(17) Krug, R. M.; Etkind, P. R. Cytoplasmic and nuclear virus-specific proteins in influenza virus-infected MDCK cells. *Virology* **1973**, *56* (1), 334–348.
(18) Murayama, R.; Harada, Y.; Shibata, T.; Kuroda, K.; Hayakawa, S.; Shimizu, K.; Tanaka, T. Influenza A virus non-structural protein 1 (NS1) interacts with cellular multifunctional protein nucleolin during infection. *Biochem. Biophys. Res. Commun.* **2007**, *362* (4), 880–885.
(19) Emmott, E.; Hiscox, J. A. Nucleolar targeting: the hub of the matter. *EMBO Rep.* **2009**, *10*, 231–238.
(20) Dove, B. K.; You, J. H.; Reed, M. L.; Emmett, S. R.; Brooks, G.; Hiscox, J. A. Changes in nucleolar morphology and proteins during infection with the coronavirus infectious bronchitis virus. *Cell. Microbiol.* **2006**, *8* (7), 1147–1157.

(21) Lam, Y. W.; Evans, V. C.; Heesom, K. J.; Lamond, A. I.; Matthews, D. A. Proteomics analysis of the nucleolus in adenovirus-infected cells. *Mol. Cell. Proteomics* **2009**, *9* (1), 117–130.

(22) Hiscox, J. A.; Whitehouse, A.; Matthews, D. A. Nucleolar proteomics and viral infection. *Proteomics* **2010**, DOI: 10.1002/pmic.201000251.

(23) Fuhrman, L. E.; Goel, A. K.; Smith, J.; Shianna, K. V.; Aballay, A. Nucleolar proteins suppress Caenorhabditis elegans innate immunity by inhibiting p53/CEP-1. *PLoS Genet.* **2009**, *5* (9), e1000657.

(24) Compans, R. W.; Dimmock, N. J. An electron microscopic study of single-cycle infection of chick embryo fibroblasts by influenza virus. *Virology* **1969**, *39* (3), 499–515.

(25) Mayer, D.; Molawi, K.; Martinez-Sobrido, L.; Ghanem, A.; Thomas, S.; Baginsky, S.; Grossmann, J.; Garcia-Sastre, A.; Schwemmle, M. Identification of cellular interaction partners of the influenza virus ribonucleoprotein complex and polymerase complex using proteomic-based approaches. *J. Proteome Res.* **2007**, *6* (2), 672–682.

(26) Melen, K.; Kinnunen, L.; Fagerlund, R.; Ikonen, N.; Twu, K. Y.; Krug, R. M.; Julkunen, I. Nuclear and nucleolar targeting of influenza A virus NS1 protein: striking differences between different virus subtypes. *J. Virol.* **2007**, *81* (11), 5995–6006.

(27) Young, J. F.; Desselberger, U.; Palese, P.; Ferguson, B.; Shatzman, A. R.; Rosenberg, M. Efficient expression of influenza virus NS1 nonstructural proteins in Escherichia coli. *Proc. Natl. Acad. Sci. U.S.A.* **1983**, *80* (19), 6105–6109.

(28) Volmer, R.; Mazel-Sanchez, B.; Volmer, C.; Soubies, S. M.; Guerin, J. L. Nucleolar localization of influenza A NS1: striking differences between mammalian and avian cells. *Virol. J.* **2010**, *7*, 63.

(29) Sheval, E. V.; Polzikov, M. A.; Olson, M. O.; Zatsepina, O. V. A higher concentration of an antigen within the nucleolus may prevent its proper recognition by specific antibodies. *Eur. J. Histochem.* **2005**, *49* (2), 117–124.

(30) DuBridge, R. B.; Tang, P.; Hsia, H. C.; Leong, P. M.; Miller, J. H.; Calos, M. P. Analysis of mutation in human cells by using an Epstein-Barr virus shuttle system. *Mol. Cell. Biol.* **1987**, *7* (1), 379–387.

(31) Carrasco, M.; Amorim, M. J.; Digard, P. Lipid raft-dependent targeting of the influenza A virus nucleoprotein to the apical plasma membrane. *Traffic* **2004**, *5* (12), 979–992.

(32) de Wit, E.; Spronken, M. I.; Bestebroer, T. M.; Rimmelzwaan, G. F.; Osterhaus, A. D.; Fouchier, R. A. Efficient generation and growth of influenza virus A/PR/8/34 from eight cDNA fragments. *Virus Res.* **2004**, *103* (1−2), 155–161.

(33) Roberts, P. C.; Compans, R. W. Host cell dependence of viral morphology. *Proc. Natl. Acad. Sci. U.S.A.* **1998**, *95* (10), 5746–5751.

(34) Simpson-Holley, M.; Ellis, D.; Fisher, D.; Elton, D.; McCauley, J.; Digard, P. A functional link between the actin cytoskeleton and lipid rafts during budding of filamentous influenza virions. *Virology* **2002**, *301* (2), 212–225.

(35) Bruce, E. A.; Medcalf, L.; Crump, C. M.; Noton, S. L.; Stuart, A. D.; Wise, H. M.; Elton, D.; Bowers, K.; Digard, P. Budding of filamentous and non-filamentous influenza A virus occurs via a VPS4 and VPS28-independent pathway. *Virology* **2009**, *390* (2), 268–278.

(36) Hutchinson, E. C.; Curran, M. D.; Read, E. K.; Gog, J. R.; Digard, P. Mutational analysis of cis-acting RNA signals in segment 7 of influenza A virus. *J. Virol.* **2008**, *82* (23), 11869–11879.

(37) Welting, T. J.; Kikkert, B. J.; van Venrooij, W. J.; Pruijn, G. J. Differential association of protein subunits with the human RNase MRP and RNase P complexes. *RNA* **2006**, *12* (7), 1373–1382.

(38) Digard, P.; Blok, V. C.; Inglis, S. C. Complex formation between influenza virus polymerase proteins expressed in Xenopus oocytes. *Virology* **1989**, *171* (1), 162–169.

(39) Elton, D.; Amorim, M. J.; Medcalf, L.; Digard, P. 'Genome gating'; polarized intranuclear trafficking of influenza virus RNPs. *Biol. Lett.* **2005**, *1* (2), 113–117.

(40) Amorim, M. J.; Read, E. K.; Dalton, R. M.; Medcalf, L.; Digard, P. Nuclear export of influenza A virus mRNAs requires ongoing RNA polymerase II activity. *Traffic* **2007**, *8* (1), 1–11.

(41) Shevchenko, A.; Wilm, M.; Vorm, O.; Mann, M. Mass spectrometric sequencing of proteins silver-stained polyacrylamide gels. *Anal. Chem.* **1996**, *68* (5), 850–858.

(42) Olsen, J. V.; de Godoy, L. M.; Li, G.; Macek, B.; Mortensen, P.; Pesch, R.; Makarov, A.; Lange, O.; Horning, S.; Mann, M. Parts per million mass accuracy on an Orbitrap mass spectrometer via lock mass injection into a C-trap. *Mol. Cell. Proteomics* **2005**, *4* (12), 2010–2021.

(43) Cox, J.; Mann, M. MaxQuant enables high peptide identification rates, individualized p.p.b.-range mass accuracies and proteome-wide protein quantification. *Nat. Biotechnol.* **2008**, *26* (12), 1367–1372.

(44) Francis, T., Jr. Transmission of Influenza by a Filterable Virus. *Science* **1934**, *80* (2081), 457–459.

(45) Emmott, E.; Rodgers, M.; Macdonald, M.; McCrory, S.; Ajuh, P.; Hiscox, J. A. Quantitative proteomics using stable isotope labeling with amino acids in cell culture (SILAC) reveals changes in the cytoplasmic, nuclear and nucleolar proteomes in Vero cells infected with the coronavirus infectious bronchitis virus. *Mol. Cell. Proteomics* **2010**, DOI: 10.1074/mcp.M900345-MCP200.

(46) Ozawa, M.; Fujii, K.; Muramoto, Y.; Yamada, S.; Yamayoshi, S.; Takada, A.; Goto, H.; Horimoto, T.; Kawaoka, Y. Contributions of two nuclear localization signals of influenza A virus nucleoprotein to viral replication. *J. Virol.* **2007**, *81* (1), 30–41.

(47) Pendle, A. F.; Clark, G. P.; Boon, R.; Lewandowska, D.; Lam, Y. W.; Andersen, J.; Mann, M.; Lamond, A. I.; Brown, J. W.; Shaw, P. J. Proteomic analysis of the Arabidopsis nucleolus suggests novel nucleolar functions. *Mol. Biol. Cell* **2005**, *16* (1), 260–269.

(48) Leung, A. K.; Andersen, J. S.; Mann, M.; Lamond, A. I. Bioinformatic analysis of the nucleolus. *Biochem. J.* **2003**, *376*, 553–569.

(49) Mann, M. Functional and quantitative proteomics using SILAC. *Nat. Rev. Mol. Cell. Biol.* **2006**, *7* (12), 952–958.

(50) Emmott, E.; Smith, C.; Emmett, S. R.; Dove, B. K.; Hiscox, J. A. Elucidation of the avian nucleolar proteome by quantitative proteomics using stable isotope labeling with amino acids in cell culture (SILAC) and alteration in the coronavirus infectious bronchitis virus infected cells. *Proteomics* **2010**, DOI: 10.1002/pmic.201000139.

(51) Jorba, N.; Juarez, S.; Torreira, E.; Gastaminza, P.; Zamarreno, N.; Albar, J. P.; Ortin, J. Analysis of the interaction of influenza virus polymerase complex with human cell factors. *Proteomics* **2008**, *8* (10), 2077–2088.

(52) Hao, L.; Sakurai, A.; Watanabe, T.; Sorensen, E.; Nidom, C. A.; Newton, M. A.; Ahlquist, P.; Kawaoka, Y. Drosophila RNAi screen identifies host genes important for influenza virus replication. *Nature* **2008**, *454* (7206), 890–893.

(53) Konig, R.; Stertz, S.; Zhou, Y.; Inoue, A.; Hoffmann, H. H.; Bhattacharyya, S.; Alamares, J. G.; Tscherne, D. M.; Ortigoza, M. B.; Liang, Y.; Gao, Q.; Andrews, S. E.; Bandyopadhyay, S.; De Jesus, P.; Tu, B. P.; Pache, L.; Shih, C.; Orth, A.; Bonamy, G.; Miraglia, L.; Ideker, T.; Garcia-Sastre, A.; Young, J. A.; Palese, P.; Shaw, M. L.; Chanda, S. K. Human host factors required for influenza virus replication. *Nature* **2010**, *463* (7282), 813–817.

(54) Brass, A. L.; Huang, I. C.; Benita, Y.; John, S. P.; Krishnan, M. N.; Feeley, E. M.; Ryan, B. J.; Weyer, J. L.; van der Weyden, L.; Fikrig, E.; Adams, D. J.; Xavier, R. J.; Farzan, M.; Elledge, S. J. The IFITM proteins mediate cellular resistance to influenza A H1N1 virus, West Nile virus, and dengue virus. *Cell* **2009**, *139* (7), 1243–1254.

(55) Karlas, A.; Machuy, N.; Shin, Y.; Pleissner, K. P.; Artarini, A.; Heuer, D.; Becker, D.; Khalil, H.; Ogilvie, L. A.; Hess, S.; Maurer, A. P.; Muller, E.; Wolff, T.; Rudel, T.; Meyer, T. F. Genome-wide RNAi screen identifies human host factors crucial for influenza virus replication. *Nature* **2010**, *463* (7282), 818–822.

(56) George, C. X.; Li, Z.; Okonski, K. M.; Toth, A. M.; Wang, Y.; Samuel, C. E. Tipping the balance: antagonism of PKR kinase and ADAR1 deaminase functions by virus gene products. *J. Interferon Cytokine Res.* **2009**, *29* (9), 477–487.

(57) Tenoever, B. R.; Ng, S. L.; Chua, M. A.; McWhirter, S. M.; Garcia-Sastre, A.; Maniatis, T. Multiple functions of the IKK-related kinase IKKepsilon in interferon-mediated antiviral immunity. *Science* **2007**, *315* (5816), 1274–1278.

(58) Ngamurulert, S.; Limjindaporn, T.; Auewaraku, P. Identification of cellular partners of Influenza A virus (H5N1) non-structural protein NS1 by yeast two-hybrid system. *Acta Virol.* **2009**, *53* (3), 153–159.

(59) Borer, R. A.; Lehner, C. F.; Eppenberger, H. M.; Nigg, E. A. Major nucleolar proteins shuttle between nucleus and cytoplasm. *Cell* **1989**, *56* (3), 379–390.

(60) Reiner, R.; Krasnov-Yoeli, N.; Dehtiar, Y.; Jarrous, N. Function and assembly of a chromatin-associated RNase P that is required for efficient transcription by RNA polymerase I. *PLoS One* **2008**, *3* (12), e4072.

(61) Jarrous, N.; Reiner, R.; Human RNase, P. a tRNA-processing enzyme and transcription factor. *Nucleic Acids Res.* **2007**, *35* (11), 3519–3524.

(62) Munday, D.; Emmott, E.; Surtees, R.; Lardeau, C.-H.; Wu, W.; Duprex, W. P.; Dove, B. K.; Barr, J. N.; Hiscox, J. A. Quantitative proteomic analysis of A549 cells infected with human respiratory syncytial virus. *Mol. Cell. Proteomics* **2010**, DOI: 10.1074/mcp.M110.001859.

(63) Reed, M. L.; Dove, B. K.; Jackson, R. M.; Collins, R.; Brooks, G.; Hiscox, J. A. Delineation and modelling of a nucleolar retention signal in the coronavirus nucleocapsid protein. *Traffic* **2006**, *7* (7), 833–848.

(64) Cawood, R.; Harrison, S. M.; Dove, B. K.; Reed, M. L.; Hiscox, J. A. Cell cycle dependent nucleolar localization of the coronavirus nucleocapsid protein. *Cell Cycle* **2007**, *6* (7), 863–867.

(65) Matthews, D. A. Adenovirus protein V induces redistribution of nucleolin and B23 from nucleolus to cytoplasm. *J. Virol.* **2001**, *75* (2), 1031–1038.

(66) Lee, T. W. R.; Lawrence, F. J.; Dauksaite, V.; Blair, G. E.; Akusjärvi, G.; Matthews, D. A. Precursor of Adenovirus core polypeptide Mu targets the nucleolus, modulates the expression of E2 proteins and alters splice site selection of E1A pre-mRNA *in vitro*. *J. Gen. Virol.* **2004**, *85*, 185–196.

(67) Lee, T. W.; Blair, G. E.; Matthews, D. A. Adenovirus core protein VII contains distinct sequences that mediate targeting to the nucleus and nucleolus, and colocalization with human chromosomes. *J. Gen. Virol.* **2003**, *84*, 3423–3428.

(68) Matthews, D. A.; Russell, W. C. Adenovirus core protein V is delivered by the invading virus to the nucleolus of the infected cell and later in infection is associated with nucleoli. *J. Gen. Virol.* **1998**, *79*, 1031–1038.

(69) Bicknell, K. A.; Brooks, G.; Kaiser, P.; Chen, H.; Dove, B. K.; Hiscox, J. A. Nucleolin is regulated both at the level of transcription and translation. *Biochem. Biophys. Res. Commun.* **2005**, *332*, 817–822.